Nuclear structure of nuclei in the ^{132}Sn mass region with $50 \leqslant Z, N \leqslant 82$

H. Zidani [*] and H. Naïdja [†]

Université Constantine 1, Laboratoire de Physique Mathématique et Subatomique (LPMPS), Constantine 25000, Algeria

(Received 28 December 2025; revised 1 April 2026; accepted 28 May 2026; published 24 June 2026)

Within the shell-model framework, we have derived a new effective interaction from the realistic N3LO interaction to provide an accurate description of the nuclear structure properties of even-even nuclei with $50 \leqslant Z$, $N \leqslant 82$, in the ^{132}Sn mass region. We validate our theoretical framework and the reliability of the new effective interaction by comparing the calculated energy levels, $E2$ transition rates, and magnetic dipole moments with experimental data. Special attention is devoted to the evolution of collectivity; an in-depth study of the quadrupole properties of different nuclei in this region reveals the presence of triaxial γ bands.

DOI: 10.1103/bd56-93q6

I. INTRODUCTION

The region around ^{132}Sn serves as a natural laboratory for exploring fundamental aspects of nuclear structure and astrophysics [1], particularly for understanding nuclear forces, shell structure, magic numbers, neutron-rich nuclei, and r-process nucleosynthesis. Experimentally, it is one of the most thoroughly studied regions, especially since the development of advanced facilities such as ISOLDE and RIKEN, which enable highly sensitive experiments involving intense beams and radioactive targets. Theoretically, it serves as a benchmark for many theoretical models, with numerous studies investigating its structure and properties.

Within the shell-model (SM) framework, part of this mass region with $Z \geqslant 50$ and $N \geqslant 82$ has long been a focus of our research. We have previously developed two effective interactions, NNS110 [2] and N3LOP [3], which have been used as references in various experimental studies [4–8].

In the present work, we extend our investigation to nuclei with $50 \leqslant Z, N \leqslant 82$, by developing a new effective interaction. This group of nuclei has been extensively studied both experimentally [9–17] and theoretically [17–25], with various spectroscopic properties (such as energy levels and half-lives) having been measured or calculated.

Theoretical studies within the SM have explored nuclei in this region using a variety of effective, phenomenological, and empirical interactions, along with different model spaces. The most well-known are the following:

(1) ^{132}Sn core: The valence space includes the $3s_{1/2}$, $2d_{5/2}$, $2d_{3/2}$, $1g_{7/2}$, and $1h_{11/2}$ orbitals; neutrons are treated as holes, while protons occupy particle orbitals [17,19,22,23].
(2) ^{100}Sn core: The valence space includes the $3s_{1/2}$, $2d_{5/2}$, $2d_{3/2}$, $1g_{7/2}$, and $1h_{11/2}$ orbitals for both neutrons and protons, which are treated as particles [18,20,21,26].
(3) ^{100}Sn core with an extended basis: The model space includes two proton orbitals ($1g_{7/2}$, $2d_{5/2}$) and eight neutron orbitals ($1g_{7/2}$, $2d_{5/2}$, $2d_{3/2}$, $3s_{1/2}$, $1h_{11/2}$, $1h_{9/2}$, $2f_{7/2}$, $3p_{3/2}$) [24].
(4) Frozen ^{78}Ni core: The model space includes all orbitals in the 28–50 major shell plus $1g_{7/2}$ and $2d_{5/2}$ for protons, and those in the 50–82 shell plus $2f_{7/2}$ and $3p_{3/2}$ for neutrons [25].

The present work aims to investigate the nuclear structure of nuclei in this mass region by developing a new effective interaction, using ^{132}Sn as a closed core.

The remainder of this paper is organized as follows. Section II details the SM calculations, including the model space and the development of the new effective interaction. Sections III–V present results concerning energy levels, $E2$ transition rates, and magnetic dipole moments, respectively, for Sn, Te, Xe, and Ba isotopes with $N \leqslant 82$, compared with experimental data. Section VI discusses the presence of quadrupole collectivity and the triaxial γ band in this mass region. Section VII provides a summary and conclusions.

II. OUTLINE OF SHELL-MODEL CALCULATIONS

A. Model space

In the present work, we study Sn, Te, Xe, and Ba isotopes with $N \leqslant 82$ using ^{132}Sn as a closed core. The model space for proton particles and neutron holes includes the $1g_{7/2}$, $2d_{5/2}$, $2d_{3/2}$, $3s_{1/2}$, and $1h_{11/2}$ orbitals. The single-particle and single-hole energies reported in Table I are taken from the experimental data of ^{133}Sb and ^{131}Sn, respectively [27]. In particular, the adopted energy levels of $\nu 1h_{11/2}$ and $\pi 3s_{1/2}$ are taken from Refs. [28] and [29], respectively.

[*] Contact author: hamad.zidani@doc.umc.edu.dz
[†] Contact author: houda.naidja@umc.edu.dz

Published by the American Physical Society under the terms of the Creative Commons Attribution 4.0 International license. Further distribution of this work must maintain attribution to the author(s) and the published article's title, journal citation, and DOI.

TABLE I. Adopted single-proton particle (ε_p) and neutron-hole (ε_n) energies (in keV). See text for details.

Orbitals	$1g_{7/2}$	$2d_{5/2}$	$2d_{3/2}$	$3s_{1/2}$	$1h_{11/2}$
ε_p	0	962	2439	2800	2791
ε_n	2434	1654	0	332	65.1

The SM calculations are performed using the Antoine SM code [30,31], with feasible M-scheme dimensions of approximately 10^{11}, which allows the inclusion of the full configurational space for all the studied nuclei except ^{128}Xe and ^{132}Ba nuclei. For these two nuclei, the size of the matrices to be set up and diagonalized is extremely large and computationally demanding. To circumvent this difficulty, we employ a truncation scheme allowing excitations of up to eight valence neutrons and protons instead of the full set of 12 valence particles. Figure 1 demonstrates an example of the convergence of our calculations in ^{132}Ba and the reliability of the adopted truncation scheme, where the results obtained with eight-particle-eight-hole (8p-8h) excitations are comparable to those including 10p-10h excitations.

B. Effective interaction

Due to the complexity of the quantum chromodynamics (QCD) (the fundamental theory of the exact strong nuclear force), effective interactions are used to approximate the exact behavior of nucleons while retaining the essential physics of the strong nuclear force. They are vital tools in theoretical nuclear physics, enabling the study and prediction of nuclear structure in a computationally manageable way.

To study nuclei in the ^{132}Sn mass region with $50 \leqslant Z$, $N \leqslant 82$, we derived a new effective interaction from the realistic N3LO potential [32], which represents a high-precision nuclear force model based on chiral effective field theory. It provides one of the most accurate and systematically improvable approaches for describing the strong interaction between nucleons, grounded in the underlying principles of QCD. The N3LO interaction reproduces nucleon-nucleon scattering

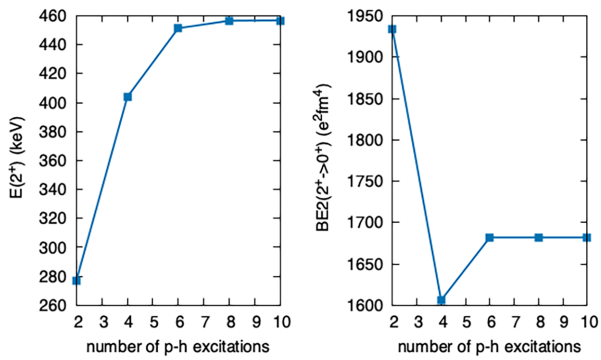


FIG. 1. The convergence of the 2^+ energy level and the $B(E2, 2^+ \rightarrow 0^+)$ transition in ^{132}Ba as a function of the number of proton-particle and neutron-hole excitations. The $B(E2, 2^+ \rightarrow 0^+)$ values are calculated using the standard effective charges ($e_\pi = 1.5e$, $e_\nu = 0.5e$).

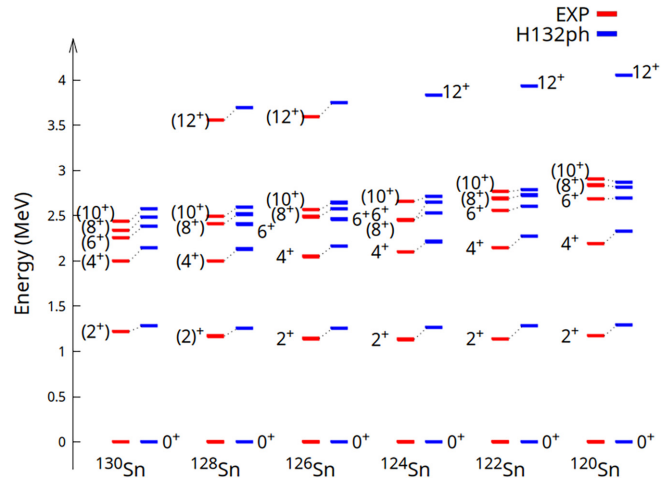


FIG. 2. Low-lying state energies of tin isotopes calculated with the H132ph effective interaction and compared with experimental data.

phase shifts and deuteron properties with very high accuracy. It is regularized with a cutoff parameter typically in the range 450–600 MeV to suppress very high-momentum components through a smooth Gaussian regulator function [32]. Although it is a low-momentum potential, its renormalization strongly reduces the dependence on the number of intermediate states included in the perturbative expansion of H_{eff}, thereby leading to a faster convergence of yrast-state energies with respect to the number of oscillator quanta, $N_{\max}$, as discussed extensively in Ref. [33].

The first step involves renormalizing the realistic interaction, where a low-momentum potential ($V_{\text{low-}k}$) [34] is derived from N3LO by taking $15\hbar\omega$ as an oscillator energy, with $\hbar\omega = 45A^{(-1/3)} - 25A^{(-2/3)}$. This is achieved by integrating the realistic potential up to a cutoff momentum $\Lambda = 2.2$ fm^{-1}, the same value used in our previous work [3]. In the second step, to make this smooth potential suitable for practical SM calculations, it is adapted to the model space using many-body perturbation theory, including all the Q-box vertex functions up to the second order of Goldstone diagrams [35]. Some two-body monopole terms ($\pi 1g_{7/2}\pi 1h_{11/2}$, $\pi 1g_{7/2}\pi 2d_{5/2}$, and $\nu 1h_{11/2}\nu 2d_{3/2}$) were slightly adjusted ($\approx$100–200 keV), to better reproduce the experimental energy levels of proton-particle ($N = 82$) and neutron-hole ($Z = 50$) nuclei. The final interaction, hereafter referred to as H132ph, is used to calculate the energy levels and electromagnetic transitions of even-even Sn, Te, Xe, and Ba isotopes with $N \leqslant 82$, as presented in the forthcoming sections.

III. ENERGY LEVELS AND WAVE-FUNCTION STRUCTURE

A. Sn isotopes

The calculated low-lying states of $^{120-130}$Sn obtained by using the H132ph effective interaction are reported in Fig. 2 and compared with experimental data. It should be noted that the spin-parity assignments of most states have not yet been confirmed experimentally. As seen in Fig. 2, the

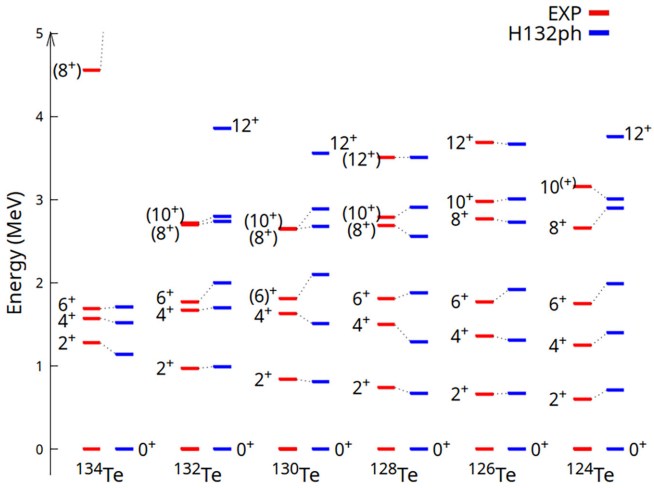


FIG. 3. Low-lying state energies of tellurium isotopes calculated with the H132ph effective interaction and compared with experimental data.

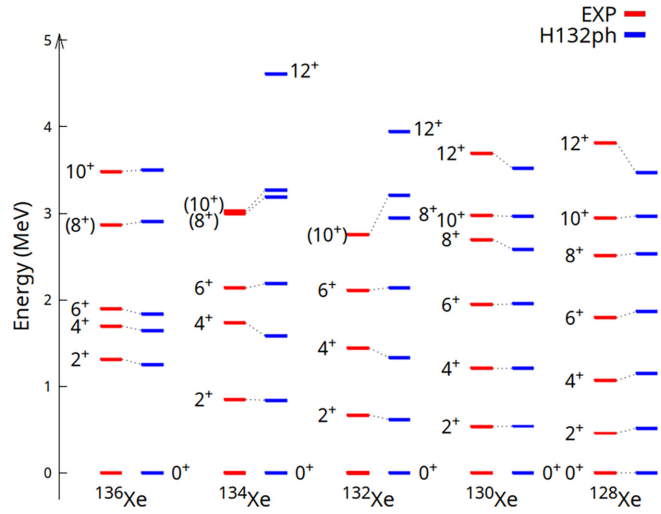


FIG. 4. Low-lying state energies of xenon isotopes calculated with the H132ph effective interaction and compared with experimental data.

calculated results show good agreement with experiment across the isotopic chain, with typical deviations ranging from a few keV to approximately 100 keV. This agreement supports the assignment of states not yet confirmed (e.g., the 10^+ state in Sn isotopes) and allows prediction of unmeasured states (e.g., the 6^+ states in ^{128,126}Sn and 12^+ levels in ^{124,122,120}Sn). Furthermore, the variation of energy levels for different states is nearly constant from ^{130}Sn to ^{120}Sn, with relatively high 2^+ excitation energies (approximately 1.2 MeV). This suggests the absence of collectivity in this isotopic chain, consistent with the proton magic number.

The wave-function (wf) structure of the ground state (g.s.) 0^+ and excited states of ^{130}Sn is dominated by the $\nu 1h^2_{11/2}$ configuration, contributing approximately 52% for the g.s., 92% for the 4^+, and 100% for the 10^+ state. This component decreases with increasing numbers of neutron holes, accompanied by the contribution of the $2d_{3/2}$ orbital in ^{128,126,124,122}Sn and the $1g_{7/2}$ orbital in ^{120}Sn. It should be noted that the coupling of the two neutron-hole orbits in our model space is insufficient to produce the 12^+ state in the ^{130}Sn nucleus.

B. Te isotopes

The calculated energy levels of Te isotopes with $72 \leqslant N \leqslant 82$, displayed in Fig. 3, show slightly poorer agreement with experimental data. In particular, the 6^+ states in $^{124–132}$Te are overestimated by approximately 200 keV, while the 4^+ states in $^{128–130}$Te are underestimated by about 100 keV. Furthermore, the calculated 8^+ and 10^+ energy levels in ^{134}Te overestimated by roughly 2 MeV are not shown in Fig. 3 to avoid compression of the energy scale for the remaining nuclei. This discrepancy can be attributed to the limited two-proton configuration space available to generate the spin-parity of these states. Some predictions also include 12^+ states in ^{132,130,124}Te. Additionally, the 2^+ excitation energy decreases from 1280 keV in ^{134}Te to 600 keV in ^{124}Te, indicating weak quadrupole correlations.

The dominant component of the wf for most low-lying states in ^{134,132,130}Te is $\pi 1g^2_{7/2} \otimes \nu 1h^n_{11/2}$ (where n denotes the number of valence neutron holes), and its contribution decreases from 98% in ^{134}Te ($n = 0$) to 15% in ^{130}Te ($n = 4$). In contrast, the 8^+ and 10^+ states in ^{130}Te, as well as the various states in ^{128,126,124}Te, are characterized by a small component (10–15%) of $\pi 1g^2_{7/2} \otimes \nu 1h^{n-2}_{11/2} 2d^2_{3/2}$, along with other smaller components.

C. Xe isotopes

The calculated energy levels of Xe isotopes, obtained using the H132ph effective interaction, are reported in Fig. 4. As shown, the calculations reproduce the experimental spectra well, particularly for the 2^+ states. Some discrepancies are observed for the 10^+ state in ^{132}Xe, which lies about 500 keV above the experimentally proposed value (2752 keV), for which the assignment is not yet confirmed. However, its energy is consistent with the confirmed experimental data for ^{136,130,128}Xe. In addition, the 12^+ state in ^{128}Xe is underestimated by approximately 300 keV compared with the experimental value, likely due to the truncation of the model space applied in this nucleus (see Sec. II A).

The wf structure in ^{136}Xe follows the same pattern as in ^{134}Te, where the 0^+, 2^+, 4^+, 6^+, and 8^+ states are dominated by a strong and nearly pure $1g^4_{7/2}$ proton configuration, whose contribution increases from about 60% in the g.s. to 90% in the 8^+ state. In contrast, the 10^+ and 12^+ states are characterized by proton excitations $1g^3_{7/2}2d_{5/2}$ and $1g^2_{7/2}1h^2_{11/2}$, respectively. The inclusion of neutron holes leads to fragmentation of the wave function, resulting in a mixing of configurations such as $\pi 1g^4_{7/2} \otimes \nu 1h^n_{11/2}$ and $\pi 1g^2_{7/2}d^2_{5/2} \otimes \nu 2d^2_{3/2}1h^{(n-2)}_{11/2}$.

D. Ba isotopes

The calculated energy levels of Ba isotopes, presented in Fig. 5, show excellent agreement with experimental data.

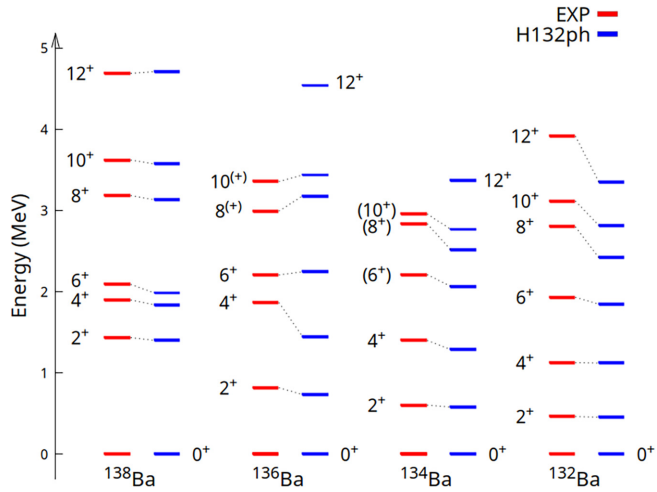


FIG. 5. Low-lying state energies of barium isotopes calculated with the H132ph effective interaction and compared with experimental data.

Some deviations are observed for (i) the 4^+ state in ^{136}Ba, which differs by about 411 keV from the experimental value, and for (ii) the 8^+ state in ^{134}Ba, which is overestimated by approximately 300 keV and is not yet experimentally confirmed. The underestimation of 8^+, 10^+, and 12^+ states in ^{132}Ba can be attributed to the truncation of the model space in this nucleus.

Turning now to the behavior of the 2^+ energy level in this isotopic chain, it decreases from 1400 keV in ^{138}Ba to 400 keV in ^{132}Ba, which may indicate the onset of quadrupole collectivity. In addition, a sudden decrease in the 12^+ energy level is observed, from 4.6 MeV in ^{136}Ba (not yet experimentally observed) to 3.4 MeV in ^{134}Ba. This behavior reflects an abrupt change in the wf configuration. In ^{136}Ba, this state is characterized by a dominant component (about 67%) of the wf $\pi 1g^6_{7/2} \otimes \nu 1h^2_{11/2}$ configuration, whereas in ^{134}Ba it becomes strongly mixed, with only about 7% contribution of the $\pi 1g^4_{7/2}2d^2_{5/2} \otimes \nu 2d^2_{3/2}1h^2_{11/2}$ configuration and additional smaller components.

In the same context, the wf structure of the g.s., as well as the 2^+ and 4^+ states in ^{138}Ba, is dominated by the $\pi 1g^6_{7/2}$ configuration. In contrast, the 6^+, 8^+, and 10^+ states are characterized by 1p-1h excitations $\pi 1g^5_{7/2}2d_{5/2}$, while the 12^+ state arises from 2p-2h excitations $\pi 1g^4_{7/2}2d^2_{5/2}$. As the number of neutron holes increases, the wave functions become more mixed, with small contributions (about 6–10%) of configurations $\pi 1g^4_{7/2}2d^2_{5/2} \otimes \nu 2d^{(n-2)}_{3/2}1h^2_{11/2}$.

IV. $B(E2; 2^+ \to 0^+)$ TRANSITIONS

Calculated $B(E2; 2^+ \to 0^+)$ transition strengths, obtained using effective charges $e_n = 0.65e$ and $e_p = 1.7e$ for neutrons and protons, respectively, are compared with experimental data [27] and, for $N = 82$, with the results obtained using our previous effective interaction N3LOP [3], which shares the same proton valence space as the new interaction H132ph.

The first notable result is that the H132ph calculations reproduce the experimental data very well within error bars, following the same systematic trend. In addition, the two SM calculations, N3LOP and H132ph, are in good agreement for all isotonic nuclei with $N = 82$. This consistency highlights the reliability of the proton-proton matrix elements in both effective interactions.

A clear difference is observed in the strength of the $B(E2; 2^+ \to 0^+)$ transitions between the Sn isotopes and the other nuclei ($Z \neq 50$). The Sn isotopes exhibit relatively small transition strengths ($\approx 400\, e^2\,\mathrm{fm}^4$), whereas significantly larger values are obtained for ^{130,128}Xe ($1500\, e^2\,\mathrm{fm}^4$) and ^{132}Ba ($1700\, e^2\,\mathrm{fm}^4$) nuclei, reflecting stronger quadrupole correlations in the latter nuclei. More details on the variation of $B(E2; 2^+ \to 0^+)$ transitions for each isotopic chain are presented in the following sections.

A. Sn isotopes

A large number of experimental studies have been carried out on the variation of the $B(E2, 2^+ \to 0^+)$ reduced transition probabilities for even-even Sn isotopes over a wide mass range. It has been observed that these $B(E2)$ values follow a parabolic trend for $A \geqslant 116$, peaking near the midshell mass number $A = 116$ [36–41]. For lighter isotopes, the experimental uncertainties suggest a rather constant behavior for $106 \leqslant A \leqslant 114$ [21,42–50], instead of the parabolic trend. Several theoretical studies have attempted to explain this asymmetry. For example, in Ref. [21], SM calculations showed that, even with an extended model space including the $1g_{9/2}$ proton orbital, deviation from the experimental data persists. The SM calculations in Refs. [50,51] indicate, within the pseudo-SU(3) symmetry framework, that the nearly constant behavior of the $B(E2)$ values is associated with quadrupole dominance, largely independent of pairing strength. In Ref. [42] α-like correlations were suggested to play an important role in explaining this feature.

The calculations presented in this work focus on the $B(E2, 2^+ \to 0^+)$ transition strength in Sn isotopes in the upper half of the major shell, namely, neutron-rich in the range $^{114-130}$Sn. The results, displayed in Fig. 6, reproduce well the general parabolic trend of the measured $B(E2, 2^+ \to 0^+)$ transition probabilities from $A = 130$ to the midshell region around $A = 116$, with a smooth increase toward the maximum. In addition, the calculations predict an approximately constant $E2$ strength at $A = 114$, whereas the experimental data indicate a slight increase, albeit with significant uncertainties.

B. Te isotopes

As shown in Fig. 6 our SM calculations performed with the H132ph effective interaction are in good agreement with experimental data for ^{134,132,130,128}Te, while a small deviation of about 10–20% is observed for ^{126,124}Te. In addition, a monotonic increase in the $B(E2)$ strength is observed along the isotopic chain with increasing neutron number, reaching relatively large values for ^{124}Te, which reflects enhanced quadrupole collectivity. Several theoretical studies,

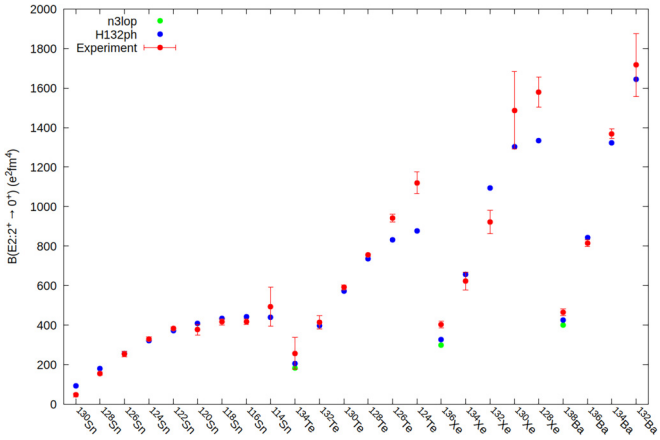


FIG. 6. $B(E2; 2^+ \rightarrow 0^+)$ transition strengths of even-even Sn, Te, Xe, and Ba isotopes with $N \leqslant 82$.

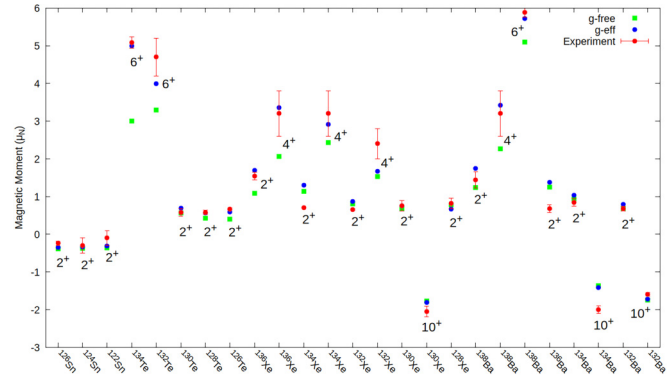


FIG. 7. Calculated magnetic dipole moments of low-lying states in Sn, Te, Xe, and Ba isotopes using free and effective g factors, compared with experimental data.

including SM calculations [52,53], the relativistic Hartree-Bogoliubov plus quadrupole collective Hamiltonian (RHB + QCH) model [54], Skyrme-Hartree-Fock (SHF) calculations within a self-consistent cranking framework [55], and quasiparticle random phase approximation (QRPA) approaches [56], predict a similar behavior of the $B(E2, 2^+ \rightarrow 0^+)$ transitions for this isotopic chain.

It is worth noting that the first excited 2^+ state in ^{136}Te lies about 370 keV lower than that in ^{132}Te; however, the $B(E2, 2^+ \rightarrow 0^+)$ value in ^{136}Te is smaller than that in ^{132}Te, which contradicts the simple systematics of quadrupole collectivity. This unusual behavior was explained in Ref. [56] by the higher neutron level density below the $N = 82$ shell gap compared to that above it, leading to a larger pairing gap that dominates over quadrupole collective effects. This high level density arises from the near degeneracy of the $1h_{11/2}$, $2d_{3/2}$, and $3s_{1/2}$ shells, along with a relatively large energy gap between the $2f_{7/2}$ and $3p_{3/2}$ shells.

C. Xe isotopes

The H132ph calculations show satisfactory agreement with the observed $B(E2, 2^+ \rightarrow 0^+)$ transition rates of the Xe isotopes, with a noticeable overestimation of about 15% in ^{128}Xe, likely due to the truncation of the model space in this nucleus. Another important feature is the rapid increase in transition strength along this isotopic chain (from 200 e^2 fm^4 in ^{134}Xe to 1600 e^2 fm^4 in ^{128}Xe), which may indicate the onset of quadrupole collectivity, as discussed in Sec. VI.

D. Ba isotopes

The variation of the $B(E2; 2^+ \rightarrow 0^+)$ transition strengths in the Ba isotopes, displayed in Fig. 6, shows excellent agreement with the experimental data across the entire isotopic chain. A noticeable increase in transition strength is observed along this chain compared to Te and Xe isotopes. In particular, the $B(E2; 2^+ \rightarrow 0^+)$ transition strength in ^{134}Ba is of the same order as that in ^{130}Xe. This behavior may be interpreted as evidence of enhanced quadrupole collectivity in Ba isotopes relative to Te and Xe isotopes.

Overall, the H132ph effective interaction reproduces the experimental $B(E2; 2^+ \rightarrow 0^+)$ transition strengths with typical deviations ranging from 2% to 20%, representing an acceptable level of shell-model accuracy for this challenging observable, which depends sensitively on the nuclear wave-function composition and the choice of effective charges.

E. Other $E2$ transitions

Other $E2$ transition strengths have been recently measured and are supported by our SM calculations. For example, the $B(E2; 6^+ \rightarrow 4^+)$ transition in ^{124}Te has been measured for the first time as 27(9) W.u. in Ref. [57], which is consistent with our SM result of 29 W.u. In addition, the lifetime measurement of the 4^+ state at 2001 keV in ^{128}Sn yields $B(E2; 4^+ \rightarrow 2^+) = 2.1(^{+2.3}_{-0.7})$ W.u. [11], in excellent agreement with our calculated value of 2.5 W.u. In contrast, the same transition in ^{132}Te, measured at 9.3(10) W.u. [58], is slightly overestimated by our calculations, which gives 13 W.u.

V. MAGNETIC DIPOLE MOMENTS μ

The magnetic dipole moment (μ) is one of the most powerful tools for investigating the structure of low-lying states. In this work, we present in Fig. 7 the μ values of various excited states for the studied nuclei, calculated using both free and effective spin and orbital g factors. The first set (free) takes the values $(g^s_\pi, g^l_\pi) = (5.586, 1.0)$ for protons and $(g^s_\nu, g^l_\nu) = (-3.826, 0.0)$ for neutrons, while the second set (effective) uses $(g^s_\pi, g^l_\pi) = (2.579, 1.004)$ for protons and $(g^s_\nu, g^l_\nu) = (-4.507, 0.057)$ for neutrons. The free g factors are determined experimentally for free nucleons, whereas the effective g factors are obtained by minimization procedures to reproduce available magnetic moment data [27].

As shown in Fig. 7, excellent agreement with experimental data is achieved when using the effective g factors, with both the sign and magnitude of the magnetic moments of low-lying states. In contrast, the agreement is significantly poorer when using the free g factors for most nuclei, which can be attributed to the absence of certain spin-orbit partners in the truncated model space. In addition, in some cases (such as the 2^+ states in Sn isotopes), the values of μ obtained with free and

TABLE II. Calculated R_{42} ratio, quadrupole properties, deformation parameters β and γ, and the experimental $R_{42\text{expt}}$ ratio in Te, Xe, and Ba isotopes.

Nucleus	$R_{42\text{expt}}$	R_{42}	$Q(2_1^+)$	$Q(2_2^+)$	$Q(3^+)$	$B(E2, 3^+ \to 2_2^+)$	β	γ
^{132}Te	1.71	1.84	−18.13	−4.84	−13.28	11.52	0.10	16.61
^{130}Te	1.94	1.85	12.79	−28.30	−1.32	649.38	0.12	19.64
^{128}Te	2.01	1.91	−42.49	26.24	−0.69	722.37	0.13	18.73
^{126}Te	2.04	1.95	−43.95	28.95	−1.49	824.60	0.14	18.95
^{124}Te	2.07	1.95	−38.72	24.93	−3.78	1000.53	0.14	20.03
^{134}Xe	2.04	1.88	−33.30	19.50	−2.16	852.38	0.12	17.48
^{132}Xe	2.16	2.17	−33.87	33.60	−0.92	1987.14	0.15	19.66
^{130}Xe	2.25	2.24	−52.13	54.73	−1.12	2362.13	0.16	18.78
^{128}Xe	2.33	2.33	−67.23	72.02	−1.87	2579.05	0.17	16.79
^{136}Ba	2.28	1.97	−54.92	5.76	75.67	0.01	0.13	16.02
^{134}Ba	2.32	2.22	−55.61	49.99	−1.50	1703.62	0.16	19.07
^{132}Ba	2.43	2.46	−56.38	52.45	−1.13	1985.04	0.18	26.02

effective g factors are very close. This can be interpreted as a consequence of the dominant neutron contribution to their wf structure, given that neutron g-factor values are similar in both sets.

Another notable feature is that most excited states exhibit positive magnetic moments. The only negative values are found for the 2^+ states in Sn isotopes and the 10^+ states in ^{130}Xe and ^{134}Ba. These negative values arise from the orientation of the magnetic moment (antialigned with the total angular momentum) and the intrinsic properties of the nucleons within the nucleus.

VI. QUADRUPOLE COLLECTIVITY

As pointed out above, the decrease in the 2^+ energy levels and the enhancement of the $B(E2; 2^+ \to 0^+)$ transition strengths observed in some isotopic chains constitute clear signatures of collective behavior. To further support our predictions regarding the presence of quadrupole correlations in this region, we present in this section additional indicators, providing more detailed information about nuclear deformation and the degree of collectivity in different nuclei.

(1) The ratio between the 4^+ and 2^+ energy levels, denoted $R_{42} = \frac{E(4^+)}{E(2^+)}$, is a simple yet powerful quantity widely used in nuclear structure studies to characterize the collective behavior of nuclei. It takes reference values of approximately 2 for a spherical vibrator, approximately 2.5 for a γ-soft nucleus, and approximately 3.33 for an axially deformed rotor.

In Table II, we observe that the calculated R_{42} ratios for different nuclei are in good agreement with the experimental data, particularly for nuclei away from $N = 82$. The obtained R_{42} values clearly indicate a predominantly spherical-collective character in tellurium isotopes, whereas the xenon and barium isotopes lie closer to the vibrational limit.

(2) Inspection of the calculated quadrupole moments in the laboratory frame for the low-lying γ band requires that $Q_s(2_\gamma^+)$ be nearly equal in magnitude and opposite in sign to $Q(2^+_{\text{yrast}})$. In addition, the quadrupole moment of the 3^+ state, $Q_s(3^+)$, should be close to zero and strongly connected to the 2_γ^+ state via an $E2$ transition. As seen from Table II, all these signatures are present in the ^{132,130,128}Xe and ^{134,132}Ba nuclei, clearly indicating the presence of low-lying γ bands, where the 2_2^+ states form the heads of the $K = 2$ γ bands. However, the absence of experimental data for quadrupole properties and $B(E2)$ transitions limits further discussion and comparison.

(3) In the Bohr-Mottelson collective model [59], the shape of a deformed nucleus is described by two parameters: β, which characterizes the magnitude of the deformation, and γ, which defines the degree of triaxiality, i.e., how far the nucleus deviates from an axially symmetric shape. The calculated values of these parameters, reported in Table II, indicate that, for most of the studied nuclei, $\beta \approx 0.1$ and $0^\circ < \gamma < 60^\circ$, clearly pointing to moderate deformation with a triaxial shape.

This behavior in Xe and Ba isotopes has already been discussed in several theoretical works. For instance, in Ref. [17], SM calculations for ^{132,134,136}Xe isotopes show an emerging collective behavior as one approaches the closed shell. The seminal paper [60] predicts low-lying collective excitations in even-even Xe isotopes using a generalized Bohr Hamiltonian approach. The interacting boson model (IBM-1) calculations in Ref. [61] identify ^{130}Xe as a strong candidate for a transitional structural shape between spherical and γ-soft configurations. In Ref. [62], results from the microscopic triaxial projected shell model (TPSM) for $^{118-128}$Xe indicate the presence of γ-soft shapes, providing evidence for triaxiality in this isotopic chain.

A similar behavior is observed in Ba isotopes: studies based on the axially deformed Woods-Saxon Hamiltonian combined with BCS pairing [63], as well as the IBM [64] and the Monte Carlo shell model (MCSM) [65,66], show a steep rise in deformation as the neutron number approaches the midshell value $N = 66$. This reflects an increase in collectivity and predicts triaxial shapes in ^{134}Ba.

VII. CONCLUSIONS

We have investigated the predictive power of the new effective interaction H132ph in describing spectroscopic

properties, considering as test cases the chain of Sn isotopes as well as their even neighbors, namely, Te, Xe, and Ba isotopes with $N \leqslant 82$. On these grounds, we conclude that the results obtained with the H132ph interaction show reasonable agreement with experimental data in reproducing low-lying energy levels, as well as $E2$ transitions and magnetic dipole moments, while also providing predictions for quantities that have not yet been observed. The results are promising and offer a solid starting point for further investigations in the ^{132}Sn mass region. Moreover, our results demonstrate good consistency between the N3LOP potential and the H132ph effective interaction in the description of the $N = 82$ isotonic chain, thus providing mutual validation of both theoretical frameworks.

In addition, to further deepen the analysis of this region, we have focused on the emergence of quadrupole collectivity by examining several indicators, which clearly point to the presence of a triaxial γ band in ^{132,130,128}Xe and ^{134,132}Ba nuclei.

Despite the fact that nuclei in this region have been extensively studied experimentally, many physical quantities remain unmeasured or insufficiently explored. In this context, our predictions may serve as a useful reference for future experimental investigations.

ACKNOWLEDGMENTS

H.N. gratefully acknowledges A. Blazhev for useful comments and discussions. This work was supported by the PRFU (Projet de Recherche Formation-Universitaire) under Contract No. B00L02UN250120220015. Computational resources were provided by the HPC facilities of UCI-UFMC and CERIST.

DATA AVAILABILITY

There are no publicly available research data or software supporting this manuscript. Requests for further information or data should be sent to the authors.

[1] O. Sorlin and M.-G, Porquet, Nuclear magic numbers: New features far from stability, Prog. Part. Nucl. Phys. **61**, 602 (2008).
[2] H. Naïdja, F. Nowacki, and K. Sieja, Recent advances in the shell model calculations of the spectroscopic properties of ^{134,136,138}Sn, Acta Phys. Pol. B **46**, 669 (2015).
[3] H. Naïdja, F. Nowacki, and B. Bounthong, Shell-model investigation of spectroscopic properties and collectivity in the nuclei beyond ^{132}Sn, Phys. Rev. C **96**, 034312 (2017).
[4] R. Lozeva *et al.*, First β-decay spectroscopy of the $^{139}_{52}$Te$_{87}$ nucleus and its P_n branching, Phys. Rev. C **110**, 064303 (2024).
[5] B. Moon *et al.*, First observation of the $\pi 0h_{11/2} \otimes \nu 0h_{9/2}$ partner orbital configuration in the odd-odd ^{138}I nucleus, Phys. Rev. C **105**, 034334 (2022).
[6] G. Häfner *et al.*, First lifetime investigations of $N > 82$ iodine isotopes: The quest for collectivity, Phys. Rev. C **104**, 014316 (2021).
[7] B. Moon *et al.*, Nuclear structure of Te isotopes beyond neutron magic number $N = 82$, Phys. Rev. C **103**, 034320 (2021).
[8] D. Rosiak *et al.*, Enhanced quadrupole and octupole strength in doubly magic ^{132}Sn, Phys. Rev. Lett. **121**, 252501 (2018).
[9] P. Guazzoni, M. Jaskola, L. Zetta, A. Covello, A. Gargano, Y. Eisermann, G. Graw, R. Hertenberger, A. Metz, F. Nuoffer, and G. Staudt, Level structure of ^{120}Sn: High resolution (p, t) reaction and shell model description, Phys. Rev. C **60**, 054603 (1999).
[10] P. Bhattacharyya, P. J. Daly, C. T. Zhang, Z. W. Grabowski, S. K. Saha, B. Fornal, R. Broda, W. Urban, I. Ahmad, D. Seweryniak, I. Wiedenhöver, M. P. Carpenter, R. V. F. Janssens, T. L. Khoo, T. Lauritsen, C. J. Lister, P. Reiter, and J. Blomqvist, Yrast excitations in $N = 81$ nuclei ^{132}Sb and ^{133}Te from ^{248}Cm fission, Phys. Rev. C **64**, 054312 (2001).
[11] M. Llanos-Expósito *et al.*, Structure of ^{128}Sn selectively populated in the β decay of the ^{128}In ground state, Phys. Rev. C **111**, 064310 (2025).
[12] J. Benito *et al.*, Detailed spectroscopy of doubly magic ^{132}Sn, Phys. Rev. C **102**, 014328 (2020).
[13] H. Suzuki *et al.*, Experimental studies of the two-step scheme with an intense radioactive ^{132}Sn beam for next-generation production of very neutron-rich nuclei, Phys. Rev. C **102**, 064615 (2020).
[14] J. Benito *et al.*, Detailed structure of ^{131}Sn populated in the β decay of isomerically purified ^{131}In states, Phys. Rev. C **110**, 014328 (2024).
[15] S. Lechner *et al.*, Electromagnetic moments of the antimony isotopes $^{112-133}$Sb, Phys. Lett. B **847**, 138278 (2023).
[16] K. Whitmore *et al.*, β decay of ^{132}In and spectroscopy of ^{132}Sn and ^{131}Sb with the GRIFFIN spectrometer, Phys. Rev. C **102**, 024327 (2020).
[17] E. E. Peters, A. E. Stuchbery, A. Chakraborty, B. P. Crider, S. F. Ashley, A. Kumar, M. T. Mc Ellistrem, F. M. Prados-Estévez, and S. W. Yates, Emerging collectivity from the nuclear structure of ^{132}Xe: Inelastic neutron scattering studies and shell-model calculations, Phys. Rev. C **99**, 064321 (2019).
[18] F. Andreozzi, L. Coraggio, A. Covello, A. Gargano, T. T. S. Kuo, and A. Porrino, Proton particle-neutron hole states in ^{132}Sb with a realistic interaction, Phys. Rev. C **59**, 746 (1999).
[19] L. Coraggio, A. Covello, A. Gargano, N. Itaco, and T. T. S. Kuo, Realistic shell-model calculations for proton particle-neutron hole nuclei around ^{132}Sn, Phys. Rev. C **66**, 064311 (2002).
[20] B. A. Brown, N. J. Stone, J. R. Stone, I. S. Towner, and M. Hjorth-Jensen, Magnetic moments of the 2^+_1 states around ^{132}Sn, Phys. Rev. C **71**, 044317 (2005).
[21] A. Banu *et al.*, ^{108}Sn studied with intermediate-energy Coulomb excitation, Phys. Rev. C **72**, 061305(R) (2005).
[22] A. Holt, T. Engeland, M. Hjorth-Jensen, and E. Osnes, Effective interactions and shell model studies of heavy tin isotopes, Nucl. Phys. A **634**, 41 (1998).
[23] E. Teruya, N. Yoshinaga, K. Higashiyama, and A. Odahara, Shell-model calculations of nuclei around mass 130, Phys. Rev. C **92**, 034320 (2015).

[24] S. Das and M. S. Sarkar, Cross-shell excitations in doubly magic ^{132}Sn and its nearest neighbours, Nucl. Phys. A **1014**, 122262 (2021).

[25] H.-K. Wang, Z.-H. Li, Y.-B. Wang, and B. Jiang, High-spin levels, β-decay and monopole effects in A = 128 hole nuclei near ^{132}Sn, Phys. Lett. B **833**, 137337 (2022).

[26] F. Andreozzi, L. Coraggio, A. Covello, A. Gargano, T. T. S. Kuo, Z. B. Li, and A. Porrino, Realistic shell-model calculations for neutron deficient Sn isotopes, Phys. Rev. C **54**, 1636 (1996).

[27] Evaluated Nuclear Structure Data File (ENSDF) database, 2025, http://www.nndc.bnl.gov/ensarchivals/.

[28] B. Fogelberg, H. Gausemel, K. A. Mezilev, P. Hoff, H. Mach, M. Sanchez-Vega, A. Lindroth, E. Ramstrom, J. Genevey, J. A. Pinston, and M. Rejmund, Decays of ^{131}In, ^{131}Sn, and the position of the $h_{11/2}$ neutron hole state, Phys. Rev. C **70**, 034312 (2004).

[29] W. Urban, W. Kurcewicz, A. Nowak, T. Rzaca-Urban, J. L. Durell, M. J. Leddy, M. A. Jones, W. R. Phillips, A. G. Smith, B. J. Varley, M. Bentaleb, E. Lubkiewicz, N. Schulz, J. Blomqvist, P. J. Daly, P. Bhattacharyya, C. T. Zhang, I. Ahmad, and L. R. Morss, Neutron single-particle energies in the ^{132}Sn region, Europhys. J. A **5**, 239 (1999).

[30] E. Caurier and F. Nowacki, Present status of shell model techniques, Acta Phys. Pol. B **30**, 705 (1999).

[31] E. Caurier, G. Martínez-Pinedo, F. Nowacki, A. Poves, and A. P. Zuker, The shell model as a unified view of nuclear structure, Rev. Mod. Phys. **77**, 427 (2005).

[32] D. R. Entem and R. Machleidt, Accurate charge-dependent nucleon-nucleon potential at fourth order of chiral perturbation theory, Phys. Rev. C **68**, 041001(R) (2003).

[33] L. Coraggio, A. Covello, A. Gargano, N. Itaco, and T. T. S. Kuo, Effective shell-model Hamiltonians from realistic nucleon-nucleon potentials within a perturbative approach, Ann. Phys. (NY) **327**, 2125 (2012).

[34] S. Bogner, T. T. S. Kuo, L. Coraggio, A. Covello, and N. Itaco, Low momentum nucleon-nucleon potential and shell model effective interactions, Phys. Rev. C **65**, 051301(R) (2002).

[35] M. Hjorth-Jensen, T. T. S. Kuo, and E. Osnes, Realistic effective interactions for nuclear systems, Phys. Rep. **261**, 125 (1995).

[36] D. C. Radford *et al.*, Nuclear structure studies with heavy neutron-rich RIBS at the HRIBF, Nucl. Phys. A **746**, 83 (2004).

[37] J. N. Orce, S. N. Choudry, B. Crider, E. Elhami, S. Mukhopadhyay, M. Scheck, M. T. McEllistrem, and S. W. Yates, $2_1^+ \to 0_1^+$ transition strengths in Sn nuclei, Phys. Rev. C **76**, 021302(R) (2007).

[38] P. Doornenbal, P. Reiter, H. Grawe, H. J. Wollersheim, P. Bednarczyk, L. Caceres, J. Cederkäll, A. Ekström, J. Gerl, M. Górska, A. Jhingan, I. Kojouharov, R. Kumar, W. Prokopowicz, H. Schaffner, and R. P. Singh, Enhanced strength of the $2_1^+ \to 0_{g.s.}^+$ transition in ^{114}Sn studied via Coulomb excitation in inverse kinematics, Phys. Rev. C **78**, 031303(R) (2008).

[39] J. M. Allmond, D. C. Radford, C. Baktash, J. C. Batchelder, A. Galindo-Uribarri, C. J. Gross, P. A. Hausladen, K. Lagergren, Y. Larochelle, E. Padilla-Rodal, and C.-H. Yu, Coulomb excitation of ^{124,126,128}Sn, Phys. Rev. C **84**, 061303(R) (2011).

[40] A. Jungclaus *et al.*, Evidence for reduced collectivity around the neutron mid-shell in the stable even-mass Sn isotopes from new lifetime measurements, Phys. Lett. B **695**, 110 (2011).

[41] G. J. Kumbartzki, N. Benczer-Koller, D. A. Torres, B. Manning, P. D. O'Malley, Y. Y. Sharon, L. Zamick, C. J. Gross, D. C. Radford, S. J. Q. Robinson, J. M. Allmond, A. E. Stuchbery, K.-H. Speidel, N. J. Stone, and C. R. Bingham, Transient field g factor and mean-life measurements with a rare isotope beam of ^{126}Sn, Phys. Rev. C **86**, 034319 (2012).

[42] C. Vaman *et al.*, $Z = 50$ shell gap near ^{100}Sn from intermediate-energy Coulomb excitations in even-mass $^{106-112}$Sn isotopes, Phys. Rev. Lett. **99**, 162501 (2007).

[43] J. Cederkäll *et al.*, Sub-barrier Coulomb excitation of ^{110}Sn and its implications for the ^{100}Sn shell closure, Phys. Rev. Lett. **98**, 172501 (2007).

[44] A. Ekström *et al.*, $0_{gs}^+ \to 2_1^+$ transition strengths in ^{106}Sn and ^{108}Sn, Phys. Rev. Lett. **101**, 012502 (2008).

[45] R. Kumar, P. Doornenbal, A. Jhingan, R. K. Bhowmik, S. Muralithar, S. Appannababu, R. Garg, J. Gerl, M. Górska, J. Kaur, I. Kojouharov, S. Mandal, S. Mukherjee, D. Siwal, A. Sharma, P. P. Singh, R. P. Singh, and H.-J. Wollersheim, Enhanced $0_{g.s.}^+ \to 2_1^+ E2$ transition strength in ^{112}Sn, Phys. Rev. C **81**, 024306 (2010).

[46] V. M. Bader, A. Gade, D. Weisshaar, B. A. Brown, T. Baugher, D. Bazin, J. S. Berryman, A. Ekström, M. Hjorth-Jensen, S. R. Stroberg, W. B. Walters, K. Wimmer, and R. Winkler, Quadrupole collectivity in neutron-deficient Sn nuclei: ^{104}Sn and the role of proton excitations, Phys. Rev. C **88**, 051301(R) (2013).

[47] P. Doornenbal, S. Takeuchi, N. Aoi, M. Matsushita, A. Obertelli, D. Steppenbeck, H. Wang, L. Audirac, H. Baba, P. Bednarczyk, S. Boissinot, M. Ciemala, A. Corsi, T. Furumoto, T. Isobe, A. Jungclaus, V. Lapoux, J. Lee, K. Matsui, T. Motobayashi, D. Nishimura, S. Ota, E. C. Pollacco, H. Sakurai, C. Santamaria, Y. Shiga, D. Sohler, and R. Taniuchi, Intermediate-energy Coulomb excitation of ^{104}Sn: Moderate $E2$ strength decrease approaching ^{100}Sn, Phys. Rev. C **90**, 061302(R) (2014).

[48] R. Kumar, M. Saxena, P. Doornenbal, A. Jhingan, A. Banerjee, R. K. Bhowmik, S. Dutt, R. Garg, C. Joshi, V. Mishra, P. J. Napiorkowski, S. Prajapati, P.-A. Söderström, N. Kumar, and H.-J. Wollersheim, No evidence of reduced collectivity in Coulomb-excited Sn isotopes, Phys. Rev. C **96**, 054318 (2017).

[49] N. Jonsson, A. Bäcklin, J. Kantele, R. Julin, M. Luontama, and A. Passoja, Collective states in even Sn nuclei, Nucl. Phys. A **371**, 333 (1981).

[50] M. Siciliano *et al.*, Pairing-quadrupole interplay in the neutron-deficient tin nuclei: First lifetime measurements of low-lying states in ^{106,108}Sn, Phys. Lett. B **806**, 135474 (2020).

[51] A. P. Zuker, Quadrupole dominance in the light Sn and in the Cd isotopes, Phys. Rev. C **103**, 024322 (2021).

[52] C. Qi, Shell-model configuration-interaction description of quadrupole collectivity in Te isotopes, Phys. Rev. C **94**, 034310 (2016).

[53] V. Kumar, P. C. Srivastava, M. J. Ermamatov, and I. O. Morales, Analysis of proton and neutron pair breakings: High-spin structures of $^{124-127}$Te isotopes, Nucl. Phys. A **942**, 1 (2015).

[54] K. Suzuki and K. Nomura, Shape transition and coexistence in Te isotopes studied with the quadrupole collective Hamiltonian based on a relativistic energy density functional, Phys. Rev. C **110**, 064304 (2024).

[55] P. Fleischer, P. Klüpfel, P.-G. Reinhard, and J. A. Maruhn, Skyrme energy functional and low lying 2^+ states in Sn, Cd, and Te isotopes, Phys. Rev. C **70**, 054321 (2004).

[56] J. Terasaki, J. Engel, W. Nazarewicz, and M. Stoitsov, Anomalous behavior of 2^+ excitations around ^{132}Sn, Phys. Rev. C **66**, 054313 (2002).

[57] M. Reece, B. J. Coombes, A. J. Mitchell, A. E. Stuchbery, G. J. Lane, A. Gargano, V. U. Bashu, L. J. Bignell, C. Gautam, L. J. McKie, N. J. Spinks, and J. A. Woodside, Coulomb excitation of ^{124}Te: Emerging collectivity and persisting seniority structure in the 6_1^+ level, Phys. Rev. C **112**, 034311 (2025).

[58] H. Mayr *et al.*, Lifetime of the 4_1^+ state of ^{132}Te, Phys. Rev. C **113**, 014318 (2026).

[59] A. Bohr and B. R. Mottelson, *Nuclear Structure* (World Scientific, Singapore, 1998), Vol. 1.

[60] L. Prochniak, K. Zajac, K. Pomorski, S. G. Rohozinski, and J. Srebrny, Collective quadrupole excitations in the $50 < Z, N < 82$ nuclei with the general Bohr Hamiltonian, Nucl. Phys. A **648**, 181 (1999).

[61] M. A. Jafarizadeh, N. Fouladi, and H. Sabri, Description of even–even $^{114-134}$Xe isotopes in the transitional region of IBM, Nucl. Phys. **43**, 34 (2013).

[62] S. Gupta, R. Bakshi, S. Singh, A. Bharti, G. H. Bhat, and J. A. Sheikh, Evolution of intrinsic nuclear structure in medium mass even-even xenon isotopes from a microscopic perspective, Chin. Phys. C **44**, 074108 (2020).

[63] M. Sugita, K. Uchiyama, and K. Furuno, Quadrupole deformation of barium isotopes, Phys. Lett. B **440**, 239 (1998).

[64] H. Sabri and M. Seidi, Energy spectra and $E2$ transition rates of $^{124-130}$Ba, Int. J. Mod. Phys. E **25**, 1650086 (2016).

[65] N. Shimizu, T. Otsuka, T. Mizusaki, and M. Honma, Monte-Carlo shell model calculations of Xe and Ba isotopes, J. Phys.: Conf. Ser. **49**, 178 (2006).

[66] N. Shimizu, T. Otsuka, T. Mizusaki, and M. Honma, Monte-Carlo shell model calculations of triaxially deformed states around ^{134}Ba, J. Phys.: Conf. Ser. **20**, 65 (2005).